

RESEARCH

Open Access



# In silico ecotoxicity assessment of photoinduced imidacloprid degradation using HPLC–HRMS, QSAR and ecotoxicity equivalents

Melanie Voigt, Victoria Langerbein and Martin Jaeger\*

## Abstract

**Background:** Imidacloprid is among the most widely used insecticides and today is found in surface and ground water worldwide. It has been registered in the EU watchlist for monitoring. To prevent imidacloprid from entering water bodies, advanced oxidation processes (AOP) have been intensely researched. Photo-irradiation proved one of the most efficient methods to degrade and eliminate anthropogenic micropollutants from waters. The ecotoxicity assessment of photoinduced degradation and transformation products especially in the absence of reference standards is still heavily explored.

**Results:** In this study, UVA and UVC irradiation in combination with titanium dioxide P25 as photocatalyst were investigated for their degrading and eliminating effects and effectiveness on imidacloprid. Humic acid was used as natural organic matter additive. High-performance liquid chromatography coupled with high-resolution mass spectrometry allowed to identify and monitor imidacloprid and its degradation intermediates yielding seven new structures and concentration–time (*c–t*) profiles. The correlation of structures and the application of radical scavengers and photocatalyst helped distinguish between direct photoinduced and indirect hydroxyl radical-induced degradation mechanisms. The identification of hydroxylated products and intermediates indicated the indirect degradation pathway, which could be suppressed by addition of a radical scavenger. The absence of hydroxylated intermediates and fragments pointed towards the direct absorption-induced degradation. Two degradation products were traced back to the direct mechanism, whereas all other products followed the indirect mechanism. The ecotoxicity of the identified compounds was assessed by quantitative structure–activity relationship (QSAR) analysis. Most products were predicted as less ecotoxic. Ecotoxicity equivalents (ETEs) were introduced allowing a classified ranking of the products and an assessment of the overall hazardous potential of the irradiated solution at a given moment. Generally, the number of hydroxyl substituents was inversely correlated to ecotoxicity. From the *c–t* curves, time-dependent ETE profiles were established.

**Conclusions:** Structure elucidation and *c–t* profiles from liquid chromatography–high-resolution mass spectrometry allowed to distinguish between direct and indirect degradation mechanisms. Structure specific ecotoxicity assessment could be achieved through QSAR analysis. Ecotoxicity hazard was ranked based on ETEs. The time-dependent

\*Correspondence: martin.jaeger@hs-niederrhein.de

Department of Chemistry and ILOC, Niederrhein University of Applied Sciences, Frankenring 20, 47798 Krefeld, Germany

ETE profile proved suitable to reflect the effect of irradiation duration and allow to estimate the irradiation time required to eliminate ecotoxicity, which may be relevant for potential applications in wastewater treatment plants.

**Keywords:** Imidacloprid, HPLC–HRMS, Ecotoxicity, QSAR, Radical scavenger, AOPs

## Background

Regular monitoring and random sampling have revealed today's ubiquity of anthropogenic micropollutants, such as pharmaceuticals or pesticides, in lakes and river waters [1–3]. This situation urged the European commission to introduce a watchlist of particularly hazardous chemical substances [4, 5]. Too little information has been available about the distribution of these substances. Each country of the European Union has hence been obliged to collect monitoring data for these substances and map their distribution and concentrations in water bodies. The current second EU watchlist comprises five neonicotinoids, among them imidacloprid [5]. Neonicotinoids are synthetic insecticides, act as neurotoxins and possess high ecotoxicity against arthropods and aquatic organisms [6]. They are also persistent and were reported to possess a half live of approximately 30 days in soils and water [7–9]. Imidacloprid occurs in European surface waters of France, Germany and Spain, but also of Australia, Brazil, Burkina Faso, China, Kenya and the USA with concentrations from  $\text{ng L}^{-1}$  to  $\mu\text{g L}^{-1}$  [10]. Agriculture and sewage systems have been recognized as main entry routes into open waters. [6]. Sewage treatment plants are no longer capable of complete elimination, as common bacterial purification were found to lack sufficient efficacy against various pharmaceuticals and pesticides [3, 11–13].

To effectively remove micropollutants, advanced treatment processes have been researched for years including Advanced Oxidation Processes (AOPs), whose common feature is the occurrence of hydroxyl radicals [14–16]. Among others, hydroxyl radicals can be generated from water through UVC irradiation [17]. Although being thus formed in low yields, hydroxyl radicals are strong oxidizing agents, their oxidation potential amounting to 2.80 V, as compared to ozone with an oxidation potential of 2.07 V [18]. In contrast, UV radiation may excite compounds directly, followed by chemical reactions.

Both pathways leading to transformation and degradation have been referred to as the direct degradation mechanism and—in case of hydroxyl radical induction—the indirect one [10, 19]. The direct mechanism is governed by the absorption spectrum of the compound and the emission spectrum of the lamp. For the generation of hydroxyl radicals UVC radiation or UVA light and a suitable photocatalyst such as titanium dioxide are required [20, 21]. Attempts were made to distinguish between both degradation mechanisms [10, 19, 22]. In

this respect, radical scavengers such as *tert*-butanol and methanol suppress hydroxyl radical-induced oxidation [23–25]. Occasionally, degradation products from AOPs were suspected to be more toxic than the original substances [26, 27]. During an AOP, the concentration–time (*c-t*) curves were often monitored and the structures of degradation or transformation products were often elucidated by high performance-liquid chromatography (HPLC) coupled to high-resolution mass spectrometry (HRMS) and higher order mass spectrometry ( $\text{MS}^n$ ) [10, 28–31]. As matrix, pure water or water containing natural organic matters such as humic acid and fulvic acid were used [32, 33].

Due to the lack of reference standards for photodegradation products, experimental determination of ecotoxicological parameters from assays with *Daphnia magna* or *Vibrio fischeri* have been rare or impossible. Quantitative Structure–Activity Relationship (QSAR) analysis is a fast and computer-based alternative for ecotoxicology assessment [34, 35]. Within QSAR, profiling is carried out first to assign the analyzed structures to a specific class, based on similarity according to the Simplified Molecular Input Line Entry Specification (SMILES) code [36]. Database comparison at this point may already yield ecotoxicological data if present. If not, two different models, that were derived from available in vitro and/or in vivo experimental data, can be employed: ECOSAR and the one introduced by Veith et al. and Pavan et al. [37, 38]. Starting from these models, chemometric methods, such as linear or non-linear regressions, are eventually used to predict the ecotoxic values for the structures under consideration.

In this study, the photoinduced degradation of imidacloprid was investigated using HPLC–HRMS and  $\text{MS}^n$ . The influence of UVA and UVC light on the degradation velocity and resulting products was studied, as well as the effects of titanium dioxide, *tert*-butanol and humic acid. The obtained *c-t* curves and molecular structures were interpreted in terms of the direct absorption-induced degradation and indirect hydroxyl radical-induced transformation. To assess ecotoxicity, the identified intermediates and products were submitted to QSAR analysis. Transformation from obtained ecotoxicity values to ecotoxicity equivalents (ETEs) for all the products led to a hazardous potential rank. The ETEs were also correlated with the *c-t* curves to yield time-dependent ETEs.

## Methods

### Chemicals and reagents

For all photoinduced degradation experiments imidacloprid ( $\geq 98.0\%$ , Sigma-Aldrich, Steinheim, Germany) was used. Imidacloprid was dissolved in ultrapure water (Berytec, Grünwald, Germany) with a final concentration of  $20 \text{ mg L}^{-1}$  ( $78 \text{ } \mu\text{mol L}^{-1}$ ), allowing for a convenient amount for characterization of degradation and transformation products. For radical scavenging experiments, *tert*-butanol (99.5%, Acros Organics, Geel, Belgium) was added to the solution to yield final concentrations of 5 vol-% ( $0.5 \text{ mol L}^{-1}$ ) and 20 vol-% ( $2 \text{ mol L}^{-1}$ ), ensuring a large excess of radical scavenger. As photocatalyst,  $100 \text{ mg L}^{-1}$  of  $\text{TiO}_2$  P25 (Acros Organics, Geel, Belgium) were suspended in the imidacloprid solution. For studying the influence of dissolved organic matter,  $5 \text{ mg L}^{-1}$  of humic acid ( $\geq 98\%$  Alfa Aesar, Haverhill, Massachusetts, USA) were added to solutions containing imidacloprid. All solution had a pH-value of  $5.0 \pm 0.5$ . As eluents for UPLC-analysis ultrapure water (A) and acetonitrile (B) (Carl Roth, Karlsruhe, Germany) were used, both acidified with 0.1% formic acid (Fluka-Honeywell; Seelze, Germany).

### Absorption spectra

For comparison of the emission of the UV lamps and the light absorption of imidacloprid, absorption spectra were recorded from 200 to 1100 nm using a UV5Nano spectrometer (Mettler Toledo, Columbus, USA). Emission spectra of the UV lamps were recorded using a HR4000 spectrometer (Ocean Optics, Duiven, The Netherlands).

### Photoinduced degradation experiments

All photoinduced degradation experiment were performed in a 1 L batchreactor (Peschl Ultraviolet, Mainz, Germany), covered with aluminum foil. Two different light sources were used: a medium-pressure mercury lamp (Heraeus, TQ 150, 150 W) for UVA radiation, that was operated with a water-cooling system, and a low-pressure mercury lamp (Heraeus TNN 15/32, 15 W) emitting UVC radiation, that was operated without cooling. Both lamps emitted polychromatic light. The maximum intensities were at 313, 365, 405, 437, 547, 578 and 580 nm. The UVC lamp emitted additionally at 185 nm and 254 nm. The total flux of photons in the wavelength range between 200 and 500 nm was determined using ferrioxalate actinometry according to IUPAC [39, 40]. The flux amounted to  $3.50 \text{ mmol min}^{-1} \text{ L}^{-1}$  for the UVA lamp and to  $2.03 \text{ mmol min}^{-1} \text{ L}^{-1}$  for the UVC lamp. The UVA lamp was allowed to reach working temperature over 2 min, while the UVC lamp did not require pre-heating. The UV lamps were inserted into the center of the reactor. A magnetic stirrer 500 rpm was used to

ensure thorough mixing in the reactor. The reaction temperature in the entire reactor amounted to  $22 \pm 2 \text{ } ^\circ\text{C}$  and was checked during the photoinduced degradation experiment using a thermometer. All solutions were irradiated for 10 min with UVA or UVC light. Samples of 2 mL were taken from the reactor at 30 s intervals during the first 5 min of irradiation and at 1-min intervals for the remaining 5 min. The samples were filtered to remove the photocatalyst from the sample and then transferred to brown glass vials so that no further reaction with light could occur. The samples were directly transferred to HPLC–HRMS analysis.

### HPLC–HRMS analysis

Reversed-phase chromatographic analysis was performed using an Eclipse Plus C18 (ZORBAX,  $3.5 \text{ } \mu\text{m}$ ,  $2.1 \times 150 \text{ mm}$ , Agilent, Waldbronn, Germany). The chromatography was performed at a flow rate of  $0.3 \text{ mL min}^{-1}$  at a column temperature of  $40 \text{ } ^\circ\text{C}$ . Elution started with eluents A and B varying from 99:1 to 70:30 within 1 min, followed by isocratic conditions A:B 25:75 during the next 10 min. At 11.1 min the solvent composition was set to 1:99 and held for 0.1 min. At minute 15 the gradient went back to the starting conditions continuing for further 15 min, amounting to a total run time of 20 min. The injection volume was  $5 \text{ } \mu\text{L}$ .

For accurate mass determination, recording of concentration–time (*c-t*) curves, and  $\text{MS}^n$  experiments, an electron spray ionization quadrupole ion trap orbitrap (ESI-Q-IT-OT) (Orbitrap IDX, ThermoFisher Scientific, Waltham, USA) coupled to an ultra-high performance liquid chromatography (UHPLC) system (Vanquish Core, ThermoFisher Scientific, Waltham, USA) was used. The mass range was set from 100 to 2000 *m/z* for all experiments. Fragmentation was performed in the higher-energy collision-induced dissociation (HCD) cell using collision energies of 30 eV for  $\text{MS}^2$  and 45 eV for  $\text{MS}^3$ . The spray voltage was set to 3500 V. The vaporizer and ion transfer tube temperature was  $300 \text{ } ^\circ\text{C}$ . For detection purposes, all ions were channeled to the orbitrap mass analyzer. The resolution was set to 60,000 for full MS, 30,000 for  $\text{MS}^2$  and 60,000 for  $\text{MS}^3$ . The mass accuracy was calibrated to 2 ppm before each experiment series. Fragmentation was analyzed manually using previous reports and strategies [41–43]. Instruments were controlled with Thermo Scientific Xcalibur Version 4.3.73.11.

### Kinetics of photodegradation

Concentration–time curves and kinetic profiles of the photoinduced degradation of imidacloprid and its transformation and degradation products were computed

using the curve fitting toolbox within the software MatLab R2018a (MathWorks, Natick, MA, USA). Mathematical treatment followed chemical kinetics as described in detail in previous studies [10, 29, 44–46].

### QSAR

The QSAR analysis was carried out *in silico* using the OECD QSAR toolbox Version 4.3.1 (OECD, Paris, France). First, the chemical structure formulae of imidacloprid and its transformation and degradation products were sketched using ACD/ChemSketch 2016.1.1 (ACD-Labs, Toronto, ON, Canada) software and imported into the QSAR toolbox. Two models were used: firstly, Ecological Structure–Activity Relationship (ECOSAR), secondly the model according to Veith et al. in its revised form by Pavan et al. [37, 38]. The acute toxicity ( $LC_{50}$ ) of *Pimephales promelas* (fathead minnow) was chosen. From the four calculation models for *P. promelas* in the QSAR toolbox the following descriptors were used. The  $\log k_{ow}$  value and the LUMO energy were applied for the first model (M1). For models 2 to 4 (M2–M4), only the  $\log k_{ow}$  value was relevant as descriptor.

Within ECOSAR, the chemical structures were employed in the SMILES representation. Depending on the SMILES combination, the chemical substances were assigned to different classes. To this purpose, a profiling was carried out to evaluate the relevant ECOSAR classes for imidacloprid and its degradation products. Suitable classes were selected for further analysis. Chronic toxicity as chronic value (ChV) and acute toxicity as lethal concentration, 50% ( $LC_{50}$ ) and half-maximal effective concentration ( $EC_{50}$ ) were predicted. As organisms, *Daphnia* (Branchiopoda), fish (Actinopterygii) and green algae were chosen.

### Time-dependent ecotoxicity equivalents

Toxicity ranking for the initial compound and the transformation and degradation products was created starting from ecotoxicity values obtained from the *in silico* QSAR analysis. A ranking was established based on these values. Subsequently, values from 1 to 17 were assigned from the least to the most toxic structure. The assigned values were multiplied by the MS peak area. The resulting values were added for all products found in the sample at a given time. Values were then normalized to the initial ecotoxicity of imidacloprid and referred to as ecotoxicity equivalents, cf. Eq. (1). Time-dependent ecotoxicity representations were obtained as the time course of the normalized values for a given sample.

### Results and discussion

It is important to prevent imidacloprid from entering surface waters to minimize its ecotoxicological hazard. With respect to researched fourth purification stages and their efficiency, the photoinduced degradation of imidacloprid was investigated and related to ecotoxicological potential. Firstly, different conditions were probed to yield a cross section of effects on photoinduced degradation. The corresponding concentration–time curves from normalized mass–area are shown in Fig. 1. For mechanistic interpretations, the UVA and UVC lamps emission spectra and the absorption spectrum of imidacloprid are given in Fig. 1 as well.

From the concentration–time profiles, it can be recognized that in general UVC radiation caused a faster and more complete degradation of imidacloprid. The additive humic acid did not have an influence on the degradation velocity, as similar rates were observed, cf. Table 1. In contrast, *tert*-butanol decelerated the degradation rate of imidacloprid. In most cases, imidacloprid

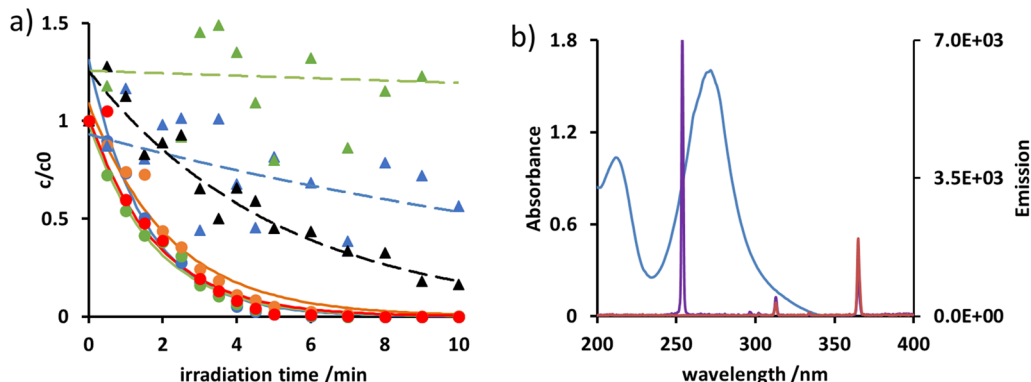


**Fig. 1** a Concentration–time curves of photoinduced imidacloprid degradation in ultrapure water (blue), in water containing *tert*-butanol 5% (green) and 20% (red), in water after addition of 100 mg  $TiO_2$  (black) and of 5 mg humic acid (orange) using a UVA lamp ( $\blacktriangle$ ) and a VUV/UVC lamp ( $\bullet$ ); b emission spectra of the UVA lamp (red), VUV/UVC lamp (violet) and absorption spectrum of imidacloprid (blue)

**Table 1** Photoinduced degradation rate constants and half-lives of imidacloprid

Irradiation source	Additives	$k/\text{min}^{-1}$	$t_{1/2}/\text{min}$
UVA	–	6.1E–02	1.1E+01
	5% <i>tert</i> -butanol	5.1E–03	1.4E+02
	100 mg TiO <sub>2</sub> P25	1.8E–01	3.9E+00
UVC	–	6.6E–01	1.1E+00
	5% <i>tert</i> -butanol	5.8E–01	1.2E+00
	20% <i>tert</i> -butanol	5.6E–01	1.2E+00
	5 mg humic acid	4.6E–01	1.5E+00

was degraded within 10 min under UVC irradiation. Under UVA irradiation, only a very weak degradation was observed. Only the addition of the photocatalyst TiO<sub>2</sub> achieved acceleration, while *tert*-butanol led to deceleration. Incomplete degradation was observed under all conditions of UVA irradiation during 10 min in contrast to UVC irradiation. Kinetic rate constants  $k$  and half-lives  $t_{1/2}$  determined from the degradation curves are collected in Table 1.

The fastest degradation was observed under VUV/UVC irradiation in pure water. The degradation rate constant was determined as 6.6E–01 min<sup>–1</sup>, which was found in a good agreement with a previous study reporting 6.7E–01 min<sup>–1</sup> [6]. The addition of *tert*-butanol and humic acid decelerated the degradation of imidacloprid only slightly. *tert*-Butanol is a known radical scavenger and as such able to intercept the hydroxyl radicals that are formed through VUV/UVC radiation. Since UVA radiation did not lead to degradation or transformation, it can be concluded that the wavelength 254 and 185 nm were essential for imidacloprid elimination [10]. As the TiO<sub>2</sub> catalyzes the formation of hydroxyl radicals under UVA irradiation, imidacloprid was found to vanish under these conditions. The contribution of hydroxyl radicals was diminished by the presence of *tert*-butanol. Despite a 25,000-fold excess, even 20% of *tert*-butanol was not sufficient to completely suppress imidacloprid elimination. It could hence be assumed that photochemistry occurred, directly induced by the absorption of radiation at 254 nm. Humic acid, which was used to simulate natural organic matter in surface water, also absorbed and thus reduced the amount of light to induce imidacloprid reactions. As a consequence, elimination by UV irradiation under non-laboratory conditions will take longer than under model conditions.

It might be concluded that degradation through hydroxyl radical formation leads to faster transformation or degradation of imidacloprid than photochemistry by direct absorption. This finding was supported,

since the addition of TiO<sub>2</sub> during UVA irradiation led to an elimination reaction constant in the same order of magnitude as during UVC irradiation, cf. Table 1.

Structural investigation of intermediates and products shall further corroborate the mechanistic findings. In addition, structure elucidation will help to assess potential hazard to the aquatic environment resulting from photo-treatment of imidacloprid.

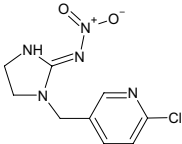
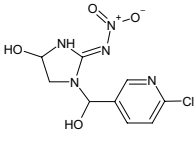
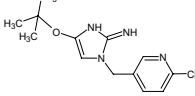
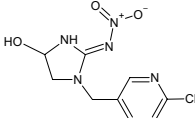
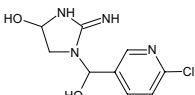
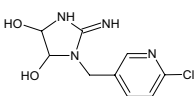
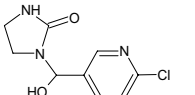
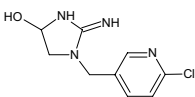
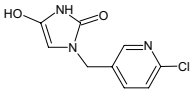
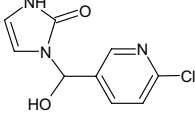
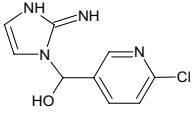
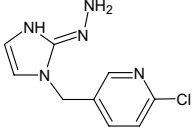
#### Identification of photoinduced degradation products

Using MS, MS/MS and MS<sup>3</sup>, structure elucidation and confirmation could be achieved. Among the photoinduced degradation and transformation products, the well-known imidacloprid derivatives 5OH-imidacloprid, desnitro-imidacloprid, desnitro-olefin-imidacloprid, urea-imidacloprid and olefin-imidacloprid were observed [47, 48]. Furthermore, some 50 products were detected upon UVC irradiation and a total of ten upon UVA irradiation. These products that occurred below 1% of the initial substance were excluded from further consideration. An overview of the most abundant products is shown in Table 2.

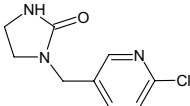
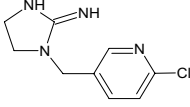
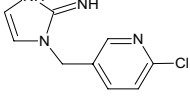
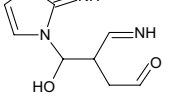
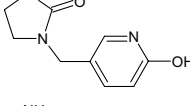
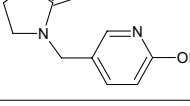
Only two of the proposed structures showed a hydroxyl group at the 6-membered ring, i.e., Imi193 and Imi194. In that case, chlorine was substituted by the hydroxyl group. All other products were hydroxylated at the imidazole ring or at the methylene group connecting the two rings, or in case of Imi288 and Imi243 at both moieties. Using MS/MS and MS<sup>3</sup>, the position of the hydroxyl group could be determined from the fragmentation pattern. Yet, regio-isomers of the imidazole ring remained undistinguishable. Examples of the MS/MS- and MS<sup>3</sup>-spectra are given for Imi226a and Imi226b in Fig. 2. As can be seen, the two Imi226 isomers exhibited the same pseudo-molecular ion  $m/z$  value with the typical chlorine isotope pattern. After collision induced dissociation, the MS/MS spectra showed an identical and a distinct fragment,  $m/z = 126$  for Imi226a and  $m/z = 126$  and 139 for Imi226b. With the help of MS<sup>3</sup>, structures could be elucidated and verified, showing that Imi226a had the hydroxyl substituent at the imidazole ring and Imi226b had it at the intermediated methylene group.

A total of 17 transformation or degradation products were identified. Five of them have not been reported before. Their fragmentation pathways are given in supplemental information, Additional file 1: Figs. S1–S7. Previous studies reported on the substance with  $m/z = 226$  but described MS<sup>n</sup> fragments different from those of this study. It can hence be assumed that these products were not identical [57]. Most of the identified products lacked the nitro group, except Imi272 and Imi288. When equal  $m/z$  values were observed at unequal retention times, e.g., Imi243a, b and Imi226a, b, the corresponding

**Table 2** Identified photoinduced degradation and transformation products of imidacloprid

Substance	RT/min	[M + H] <sup>+</sup> <sub>exact</sub>	[M + H] <sup>+</sup> <sub>accurate</sub>	Δ ppm	Proposed structure	References
Imidacloprid	5.82	256.0596	256.0594	0.78		
Imi288	5.34	288.0494	288.0500	2.08		[47, 49–52]
Imi281	4.75	281.1163	281.1166	1.07		This study
Imi272	5.00	272.0545	272.0546	0.37		[47, 51–57]
Imi243a	3.79	243.0643	243.0640	1.23		This study
Imi243b	3.95	243.0643	243.0642	0.41		This study
Imi228	4.79	228.0534	228.0531	1.32		[56, 58]
Imi227	4.14	227.0694	227.0695	0.44		[48]
Imi226a	4.88	226.0378	226.0376	0.88		This study
Imi226b	4.80	226.0378	226.0375	1.33		This study
Imi225	4.29	225.0538	225.0539	0.44		This study
Imi224	3.82	224.0697	224.0701	1.79		[49]

**Table 2** (continued)

Substance	RT/min	[M + H] <sup>+</sup> <sub>exact</sub>	[M + H] <sup>+</sup> <sub>accurate</sub>	Δ ppm	Proposed structure	References
Imidacloprid-urea	4.22	212.0585	212.0586	0.47		[47–49, 51–54, 56, 59–69]
Desnitro-imidacloprid	4.79	211.0745	211.0743	0.95		[47–49, 52, 60, 61, 65, 67, 69]
Desnitro-olefin-imidacloprid	4.01	209.0589	209.0593	0.48		[47, 48, 54, 57]
Imi197	1.30	197.1033	197.1034	0.51		This study
Imi194	3.98	194.0924	194.0923	0.52		[48]
Imi193	2.00	193.1084	193.1082	1.04		[48]

compounds were interpreted as regio-isomers with the hydroxyl group at different positions. The product Imi281 was only observed in the presence of *tert*-butanol and could be characterized by MS/MS as desnitro-olefin-imidacloprid *tert*-butyl ether, cf. Table 2.

In order to relate products to either the hydroxyl mechanism or the direct absorption mechanism, it is also interesting to classify the products to the conditions of the experiment. The classification and values referring to the percentage of the maximum of the *c-t* curve relative to the initial imidacloprid concentration are collected in Table 3. Concentration–time curves were recorded for all products. They are exemplarily shown for desnitro-imidacloprid and Imi194 in Fig. 2.

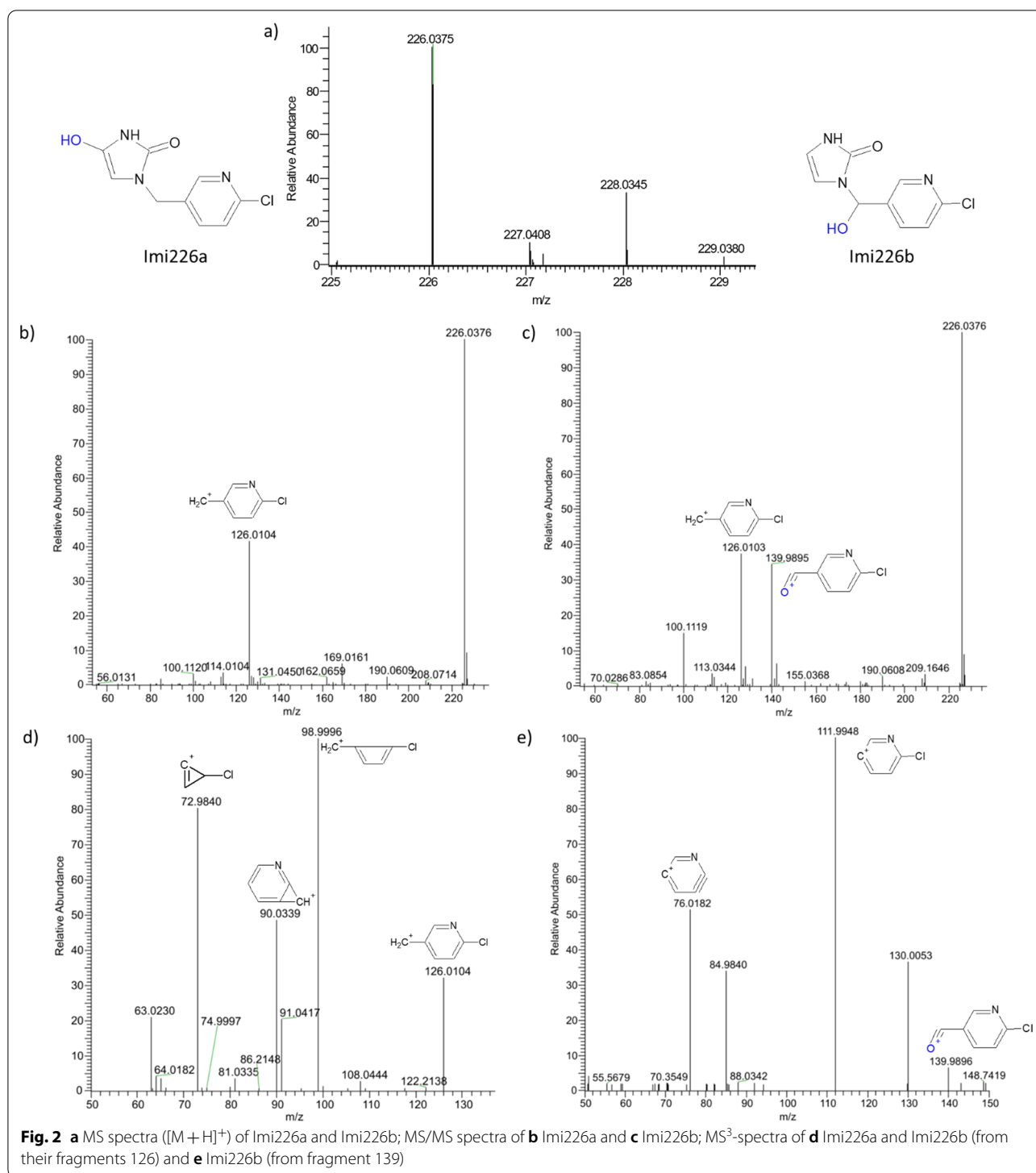
In case of UVA irradiation in the absence of TiO<sub>2</sub>, only two products were identified with a proportion of more than 1%: desnitro-imidacloprid and desnitro-olefin-imidacloprid. Hence, these products should originate from direct absorption of UVA radiation and subsequent reactions. The lack of hydroxyl radical generating radiation led to the absence of the indirectly formed products, such as Imi227. Since imidacloprid was degraded only very little, few products at small abundance were expected.

In the presence of TiO<sub>2</sub>, 4 products could be identified: Imi288, Imi272, Imi243a and Imi243b. From their

chemical structure, it can be deduced that these transformation products involved hydroxyl substitution favored through the presence of photocatalyst.

Further products originated from VUV/UVC irradiation. The products Imi193, Imi194, imidacloprid-urea, Imi224, and Imi227 could be observed under all VUV/UVC irradiation conditions. Interestingly, the formation of the urea derivative seemed a consequence of UVC irradiation, under both hydroxyl radical formation and radical suppression conditions. Since the urea derivative did not occur under UVA irradiation in the presence of photocatalyst, distinction between the two mechanisms was not possible. The loss of the nitro group was found for a variety of conditions. The proportion of Imi193, Imi194, imidacloprid-urea, Imi224 and Imi227 decreased upon addition of more *tert*-butanol due to its radical scavenging capability.

The products Imi243, Imi226a, Imi226b and desnitro-olefin-imidacloprid were only observed in the absence of *tert*-butanol. These products hence stemmed from hydroxyl radical reactions. Addition of radical scavenger suppressed their formation as well. Yet, desnitro-imidacloprid, Imi225 and Imi197 were still observed at 5% *tert*-butanol, but disappeared at 20% *tert*-butanol. Desnitro-imidacloprid was likely to be formed via the



direct mechanism as well, while 5% *tert*-butanol was sufficient to hamper the formation of Imi225, which possess the hydroxylated methylene moiety and was hence considered due to the indirect mechanism. The higher content of *tert*-butanol eventually suppressed its formation.

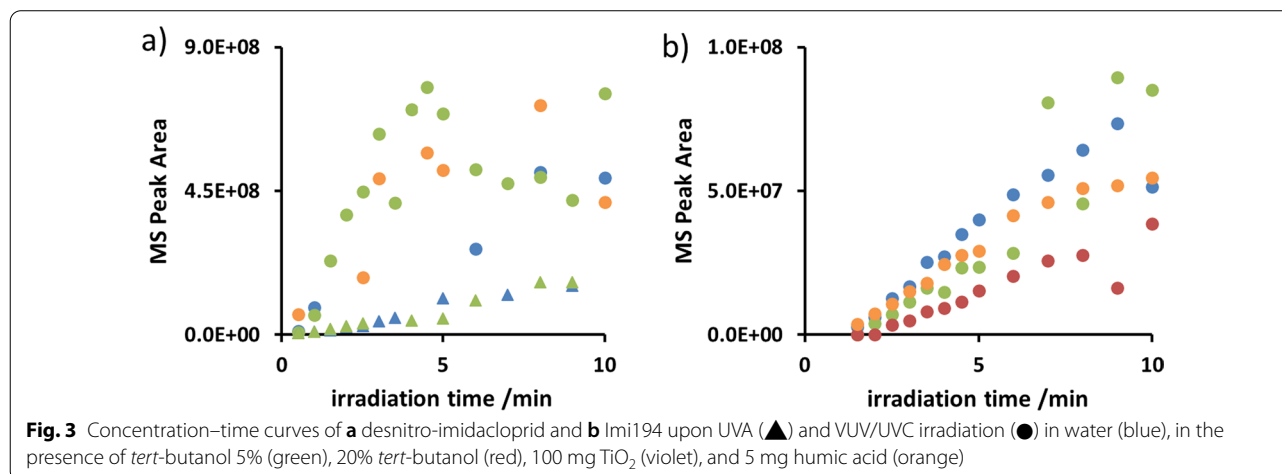
The presence of *tert*-butanol caused the occurrence of desnitro-olefin-imidazole-butyl ether Imi281, its proportion increasing with increasing amount of *tert*-butanol.

The concentration–time curves of Imi194 and desnitro-imidacloprid are presented in Fig. 3. The



**Table 3** Photoinduced degradation and transformation products of imidacloprid under different conditions; values refer to the percentage of the maximum of the *c-t* curve relative to initial imidacloprid concentration

Substance	UVA /%	UVA + 5% <i>tert</i> -butanol/%	UVA + TiO <sub>2</sub> P25/%	UVC/%	UVC + 5 mg humic acid/%	UVC + 5% <i>tert</i> -butanol/%	UVC + 20% <i>tert</i> -butanol/%
Imidacloprid	X	X	X	X	X	X	X
Imi288			1.8				
Imi281						6.3	9.3
Imi272			7.6				
Imi243a			1.4	1.4	1.5		
Imi243b			2.5				
Imi228				4.2	5.5		
Imi227				26.1	20.8	22.8	8.16
Imi226a				2.3	5.0		
Imi226b				1.0	1.7		
Imi225				2.3	2.3	8.9	
Imi224				2.1	6.7	8.4	2.3
Imidacloprid-urea				48.8	67.8	90.8	40.4
Desnitro-imidacloprid	6.1	7.0		21.4	39.6	64.6	
Desnitro-olefin-imidacloprid	7.0	6.7		4.2	4.7		
Imi197				1.2	1.8	2.1	
Imi194				3.1	3.0	7.5	1.5
Imi193				2.8	2.4	6.6	1.4



profiles illustrate the different formation kinetics of the secondary products. The course of desnitro-imidacloprid was followed during UVA irradiation in water with 5% *tert*-butanol, during UVC irradiation in water, in water with 5% and 20% *tert*-butanol and in the presence of humic acid.

Degradation or transformation products whose *c-t* curves still increased after 10 min of UV exposure, such as Imi193 and Imi194, were observed. Other

transformation products that were degraded again, such as the products Imi225 and Imi227, were found as well. They could be described as follow-up and subsequent follow-up products.

#### In silico assessment of ecotoxicity

The structures identified and illustrated in Table 2 were used for the QSAR analysis. For the QSAR analysis based on ECOSAR, profiling yielded the structural

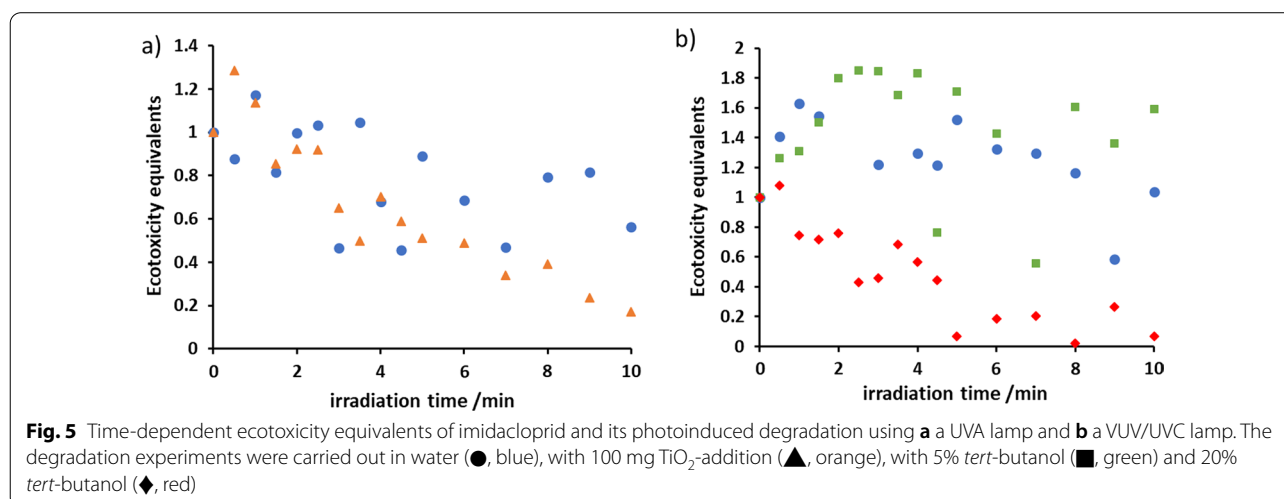
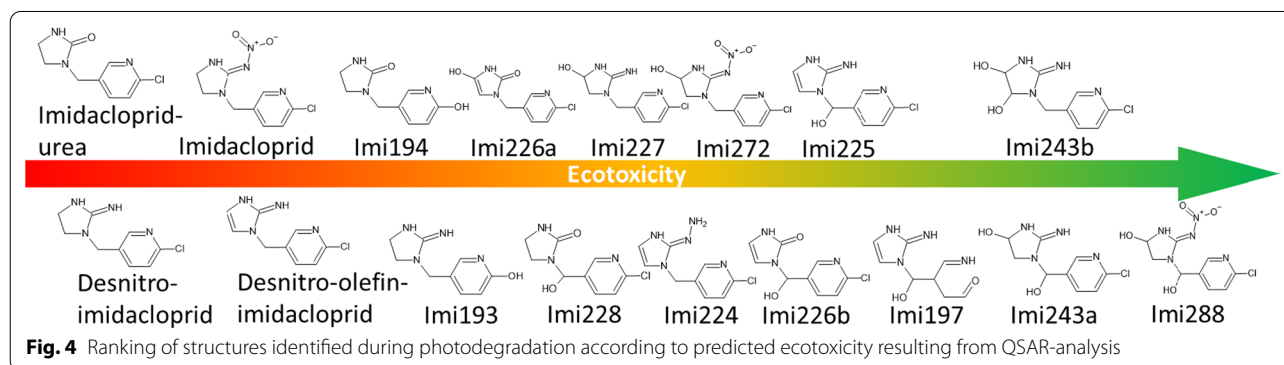
classification. Best results were suggested when using the classes aliphatic amines and halopyridines, see Additional file 1: Table S2. The QSAR analysis was performed and ecotoxicity predicted. The resulting values are collected in Additional file 1: Table S3. The butyl-ether Imi281 was rated most ecotoxic from the prediction, see Additional file 1: Table S3. However, this product was only formed in the presence of *tert*-butanol and was hence excluded from further ecotoxicity assessment.

A ranking of the identified structures of Table 2 according to ecotoxicity is displayed in Fig. 4.

Among the imidacloprid transformation and degradation products, imidacloprid-urea, desnitro-imidacloprid, desnitro-olefin-imidacloprid and imidacloprid as initial compound were ranked as the most ecotoxic substances against organisms from the aquatic environment. These compounds were not hydroxylated, but were detected under hydroxyl radical generating conditions, cf. Table 3 and above. Imidacloprid-urea was formed only during UVC irradiation. Its degradation was hampered in the presence of radical scavengers. The observation suggests that degradation was favored by hydroxyl radicals.

In combination with the QSAR results, it might be concluded that ecotoxic effects could be reduced through hydroxyl substituents and secondary product elimination by hydroxyl radicals. While the compounds Imi226a and 226b demonstrate that the position of the hydroxyl group may play a decisive role for the ecotoxicity of mono-hydroxylated products, the di-hydroxylated Imi243a and Imi243b were rated equally ecotoxic. A hydroxyl group at the azole ring generally led to higher ecotoxicity than at the methylene moiety. Hydroxyl substitution of the chlorine hence a hydroxylated pyridine ring, cf. Imi193 and Imi194, was predicted to be again more ecotoxic than azole hydroxylation. In case of Imi243a and Imi243b being hydroxylated azole regio-isomers, the position was not given importance with respect to aquatic hazard potential. Therefore, no further distinction was made for these derivatives. As mentioned, the number of hydroxyl substituents exercised a positive effect: the more hydroxyl groups the less ecotoxic the transformation product was predicted.

Up to this point, the ecotoxicity was computed for each compound separately. Yet, the ecotoxicity is a function



of irradiation time when conditions are kept constant. Hence, the total ecotoxicity of the solution was considered and computed as ecotoxicity equivalents (*ETE*) that are a function of irradiation time, cf. Equation 1 and Fig. 5:

$$ETE(t) = \left[ \sum_{n=1}^n (EQ * MS \text{ Peak Area}_A) \right] (t) / ETE(t=0), \quad (1)$$

where  $n$  is the number of identified products including imidacloprid,  $EQ$  the ecotoxicity ranking value resulting from QSAR analysis and  $t$  the irradiation time. The value of  $ETE(t=0)$  equals the QSAR value of imidacloprid.

As can be seen from Fig. 5, UVA irradiation induced a steady decrease of ecotoxicity. Since only few degradation and transformation products were formed during UVA irradiation and their MS peak area remained very small as compared to that of imidacloprid, the predicted ecotoxicity resulted predominantly from imidacloprid. The *ETE* time-dependence equaled the degradation profile of imidacloprid, cf. Fig. 5a. Upon addition of  $TiO_2$ , *ETEs* decayed faster, as was observed for imidacloprid as well.

Under VUV/UVC irradiation, the ecotoxicity initially increased both for imidacloprid in pure water and in the presence of 5% *tert*-butanol. The most transformation and degradation products were observed under these conditions; the profile of the ecotoxicity–time curves reflected the profile of the total product formation. At first, the ecotoxicity increased slowly, as did the number of observed products. Then, it decreased in the same way the products were eliminated again due to continuing VUV/UVC radiation. When the *tert*-butanol concentration amounted to 20%, the overall ecotoxicity decreased with irradiation time, since significantly fewer products were formed. Hence, imidacloprid had the greatest impact on the ecotoxicity under these conditions. The lowest overall ecotoxicity expressed in *ETEs* was achieved using UVA irradiation in the presence of 100 mg  $TiO_2$  or using VUV/UVC irradiation in the presence of 20% *tert*-butanol.

The findings emphasize the importance of monitoring secondary products during UV irradiation. Too short a treatment might yield a mixture of intermediate products that might prove more ecotoxic than the initial substance. Using HRMS as detector, structural information could be obtained and used further for ecotoxicity prediction by QSAR. Monitoring all compounds was easily achieved by HRMS as well. Introducing ecotoxicity equivalents, the ecotoxicity of the total solution exposed to irradiation under different conditions could be assessed. These time-dependent *ETEs* could help better estimate efficacy and treatment times for elimination of hazardous substances.

## Conclusions

The elimination of imidacloprid from model waters was accomplished through irradiation with UVC radiation and UVA light in the presence of the photocatalyst  $TiO_2$  P25. Using HPLC–HRMS and MS<sup>3</sup>, the degradation was monitored as  $c$ - $t$  curves and the degradation and transformation products structurally characterized leading to the discovery of seven new transformation products. Degradation was traced back to the direct photoinduced, e.g., desnitro-imidacloprid, and the indirect hydroxyl radical-induced mechanism, e.g., Imi227, as supported by the identified structures. The distinction was supported by the experimental conditions, in particular presence and absence of  $TiO_2$  during UVA irradiation and the scavenging of hydroxyl radicals by *tert*-butanol. Ecotoxicity was assessed by means of QSAR analysis based on the elucidated secondary products. Increasing number of hydroxyl groups due to the indirect mechanism and cleavage of the chlorine substituent were found to decrease ecotoxicity. Ecotoxicity values from QSAR were transformed into *ETEs* and an ecotoxicity ranking was established. Since transformation and degradation products were exposed to radiation and thus continued to react, time-dependent *ETEs* were introduced to reflect the overall ecotoxicity of the solution at a given moment. The *ETE*–time curve suggested an initial increase of ecotoxicity of an imidacloprid solution upon UVC irradiation followed by a significant removal, while UVA exposure led to a steady decrease. Irradiation times necessary for elimination may be better estimated from time-dependent *ETEs*. The presence of humic acid as NOM showed that irradiation with and without photocatalyst under real conditions would require longer duration, but would still lead to successful degradation. While UVC irradiation is a well-established method for the treatment of drinking water, large-scale waste water treatment using UVC or photocatalyst enhanced UVA light will prove difficult due to the need for effective light penetration. While energy consumption might be reduced by using light-emitting diodes, a sufficiently long irradiation time has to be ensured. Yet, the degradation efficiency and the predicted low environmental hazardous potential suggest UV irradiation may be also a promising waste water treatment methodology.

## Abbreviations

AOPs: Advanced oxidation processes; ChV: Chronic value; ECOSAR: Ecological structure–activity relationships; ESI-Q-IT-OT: Electron spray ionization quadrupole ion trap orbitrap; EU: European Union;  $c$ - $t$ : Concentration–time;  $EC_{50}$ : Half-maximal effective concentration; *ETE*: Ecotoxicity equivalents; HCD: Higher-energy collision-induced dissociation; HPLC–HRMS: High-performance liquid chromatography–high-resolution mass spectrometry; LC50: Lethal concentration; LUMO: Lowest unoccupied molecular orbital; OECD: Organisation

for Economic Co-operation and Development; QSAR: Quantitative structure–activity relationship; SMILES: Simplified molecular input line entry specification; UHPLC: Ultra-high performance liquid chromatography; UV: Ultraviolet; VUV: Vacuum-UV.

## Supplementary Information

The online version contains supplementary material available at <https://doi.org/10.1186/s12302-022-00616-0>.

**Additional file 1: Table S1.** Imidacloprid and its photoinduced degradation products: Retention times  $R_t$  and observed higher order MS fragments. **Figure S1.** Fragmentation pathway of Imi197. **Figure S2.** Fragmentation pathway of Imi225. **Figure S3.** Fragmentation pathway of Imi226a. **Figure S4.** Fragmentation pathway of Imi226b. **Figure S5.** Fragmentation pathway of Imi243a. **Figure S6.** Fragmentation pathway of Imi243b. **Figure S7.** Fragmentation pathway of Imi281. **Table S2.** Profiling of imidacloprid and its photoinduced transformation and degradation products. **Table S3.** QSAR analysis of imidacloprid and its photoinduced transformation and degradation products.

### Acknowledgements

The authors are grateful to Joachim Horst for technical support.

### Author contributions

MV: conceptualization, validation, data curation, experiments, writing—original draft VL: data curation, preparation, experiments MJ: formal analysis, writing—review and editing, supervision. All authors read and approved the final manuscript.

### Funding

Open Access funding enabled and organized by Projekt DEAL. Open access funding provided by Niederrhein University of Applied Sciences.

### Availability of data and materials

Data can be obtained upon request from the corresponding author. They will be made available via a link to the cloud Sciebo.

### Declarations

#### Ethics approval and consent to participate

Not applicable.

#### Consent for publication

Not applicable.

#### Competing interests

The authors declare that they have no competing interests.

Received: 2 December 2021 Accepted: 31 March 2022

Published online: 26 May 2022

## References

- Kümmerer K (2009) Antibiotics in the aquatic environment—a review—part I. *Chemosphere* 75:417–434. <https://doi.org/10.1016/j.chemosphere.2008.11.086>
- Syafurudin M, Kristanti RA, Yuniarto A et al (2021) Pesticides in drinking water—a review. *Int J Environ Res Public Health* 18:468. <https://doi.org/10.3390/ijerph18020468>
- Pietrzak D, Kania J, Malina G et al (2019) Pesticides from the EU first and second watch lists in the water environment. *Clean—Soil Air Water*. <https://doi.org/10.1002/clen.201800376>
- European Union (2015) Commission Implementing Decision (EU) 2015/495 establishing a watch list of substances for Union-wide monitoring in the field of water policy pursuant to Directive 2008/105/EC of the European Parliament and of the Council. *Off J Eur Union*, L 78/40–42, 24.3.2015. [http://data.europa.eu/eli/dec\\_impl/2015/495/oj](http://data.europa.eu/eli/dec_impl/2015/495/oj)
- European Union (2018) Commission Implementing Decision (EU) 2018/840 of 5 June 2018 establishing a watch list of substances for Union-wide monitoring in the field of water policy pursuant to Directive 2008/105/EC of the European Parliament and of the Council and repealing Commission Implementing Decision (EU) 2015/495 (notified under document C(2018) 3362). *Off J Eur Union*, L 141/9, 7.6.2018. [http://data.europa.eu/eli/dec\\_impl/2018/840/oj](http://data.europa.eu/eli/dec_impl/2018/840/oj)
- Goulson D (2013) An overview of the environmental risks posed by neonicotinoid insecticides. *J Appl Ecol* 50:977–987. <https://doi.org/10.1111/1365-2664.12111>
- Sarkar MA, Roy S, Kole RK, Chowdhury A (2001) Persistence and metabolism of imidacloprid in different soils of West Bengal. *Pest Manag Sci* 57:598–602. <https://doi.org/10.1002/ps.328>
- Sarkar MA, Biswas PK, Roy S et al (1999) Effect of pH and type of formulation on the persistence of imidacloprid in water. *Bull Environ Contam Toxicol* 63:604–609. <https://doi.org/10.1007/s001289901023>
- Anderson JC, Dubetz C, Palace VP (2015) Neonicotinoids in the Canadian aquatic environment: a literature review on current use products with a focus on fate, exposure, and biological effects. *Sci Total Environ* 505:409–422. <https://doi.org/10.1016/j.scitotenv.2014.09.090>
- Voigt M, Jaeger M (2021) Structure and QSAR analysis of photoinduced transformation products of neonicotinoids from EU watchlist for ecotoxicological assessment. *Sci Total Environ* 751:141634. <https://doi.org/10.1016/j.scitotenv.2020.141634>
- Yi X, Zhang C, Liu H et al (2019) Occurrence and distribution of neonicotinoid insecticides in surface water and sediment of the Guangzhou section of the Pearl River, South China. *Environ Pollut* 251:892–900. <https://doi.org/10.1016/j.envpol.2019.05.062>
- Barbosa MO, Moreira NFF, Ribeiro AR et al (2016) Occurrence and removal of organic micropollutants: an overview of the watch list of EU decision 2015/495. *Water Res* 94:257–279. <https://doi.org/10.1016/j.watres.2016.02.047>
- Sousa JCG, Ribeiro AR, Barbosa MO et al (2018) A review on environmental monitoring of water organic pollutants identified by EU guidelines. *J Hazard Mater* 344:146–162. <https://doi.org/10.1016/j.jhazmat.2017.09.058>
- Coha M, Farinelli G, Tiraferri A et al (2021) Advanced oxidation processes in the removal of organic substances from produced water: Potential, configurations, and research needs. *Chem Eng J* 414:128668. <https://doi.org/10.1016/j.cej.2021.128668>
- Mazivila SJ, Ricardo IA, Leitão JMM, Esteves da Silva JCG (2019) A review on advanced oxidation processes: From classical to new perspectives coupled to two- and multi-way calibration strategies to monitor degradation of contaminants in environmental samples. *Trends Environ Anal Chem* 24:1–10. <https://doi.org/10.1016/j.teac.2019.e00072>
- Deng Y, Zhao R (2015) Advanced oxidation processes (AOPs) in wastewater treatment. *Curr Pollut Reports* 1:167–176. <https://doi.org/10.1007/s40726-015-0015-z>
- Zoschke K, Börnick H, Worch E (2014) Vacuum-UV radiation at 185 nm in water treatment—a review. *Water Res* 52:131–145. <https://doi.org/10.1016/j.watres.2013.12.034>
- Sillanpää M (2020) *Advanced water treatment—advanced oxidation process*. Elsevier, Amsterdam
- Zhang Y, Zhang J, Xiao Y et al (2017) Direct and indirect photodegradation pathways of cytostatic drugs under UV germicidal irradiation: process kinetics and influences of water matrix species and oxidant dosing. *J Hazard Mater* 324:481–488. <https://doi.org/10.1016/j.jhazmat.2016.11.016>
- Chávez AM, Ribeiro AR, Moreira NFF et al (2019) Removal of organic micropollutants from a municipal wastewater secondary effluent by UVA-LED photocatalytic ozonation. *Catalysts*. <https://doi.org/10.3390/catal9050472>
- Al-Mamun MR, Kader S, Islam MS, Khan MZH (2019) Photocatalytic activity improvement and application of UV-TiO<sub>2</sub> photocatalysis in textile wastewater treatment: a review. *J Environ Chem Eng*. <https://doi.org/10.1016/j.jece.2019.103248>
- Hensen B, Olsson O, Kümmerer K (2019) The role of irradiation source setups and indirect phototransformation: kinetic aspects and the formation of transformation products of weakly sunlight-absorbing pesticides. *Sci Total Environ* 695:133808. <https://doi.org/10.1016/j.scitotenv.2019.133808>
- Kozmér Z, Takács E, Wojnárovits L et al (2016) The influence of radical transfer and scavenger materials in various concentrations on the

- gamma radiolysis of phenol. *Radiat Phys Chem* 124:52–57. <https://doi.org/10.1016/j.radphyschem.2015.12.011>
24. Wirzberger V, Klein M, Woermann M et al (2021) Matrix composition during ozonation of N-containing substances may influence the acute toxicity towards *Daphnia magna*. *Sci Total Environ* 765:142727. <https://doi.org/10.1016/j.scitotenv.2020.142727>
  25. von Piechowski M, Thelen M-A, Hoigne J, Bühler RE (1992) Tert-butanol as an OH-scavenger in the pulse radiolysis of oxygenated aqueous systems. *Ber Bunsenges Phys Chem* 96:1448–1454
  26. Fatta-Kassinos D, Vasquez MI, Kümmerer K (2011) Transformation products of pharmaceuticals in surface waters and wastewater formed during photolysis and advanced oxidation processes—degradation, elucidation of byproducts and assessment of their biological potency. *Chemosphere* 85:693–709. <https://doi.org/10.1016/j.chemosphere.2011.06.082>
  27. Vasconcelos TG, Henriques DM, König A et al (2009) Photo-degradation of the antimicrobial ciprofloxacin at high pH: identification and biodegradability assessment of the primary by-products. *Chemosphere* 76:487–493. <https://doi.org/10.1016/j.chemosphere.2009.03.022>
  28. Voigt M, Bartels I, Schmiemann D et al (2021) Metoprolol and its degradation and transformation products using aops-assessment of aquatic ecotoxicity using qsar. *Molecules*. <https://doi.org/10.3390/molecules26113102>
  29. Voigt M, Hentschel B, Theiss N et al (2020) Lomefloxacin—occurrence in the German River Erf, its photo-induced elimination, and assessment of ecotoxicity. *Clean Technol* 2:74–90. <https://doi.org/10.3390/cleantechnol2010006>
  30. Afonso-Olivares C, Montesdeoca-Esponda S, Sosa-Ferrera Z, Santana-Rodríguez JJ (2016) Analytical tools employed to determine pharmaceutical compounds in wastewaters after application of advanced oxidation processes. *Environ Sci Pollut Res* 23:24476–24494. <https://doi.org/10.1007/s11356-016-7325-6>
  31. Picó Y, Barceló D (2015) Transformation products of emerging contaminants in the environment and high-resolution mass spectrometry: a new horizon. *Anal Bioanal Chem* 407:6257–6273. <https://doi.org/10.1007/s00216-015-8739-6>
  32. Slomberg DL, Ollivier P, Radakovitch O et al (2017) Insights into natural organic matter and pesticide characterisation and distribution in the Rhone River. *Environ Chem* 14:64–73. <https://doi.org/10.1071/EN16038>
  33. Uyguner CS, Bekbolet M, Swietlik J (2006) Natural organic matter: definitions and characterization. In: *Control disinfect by-products drink water system*. Nova Publishers, Hauppauge, NY, pp 253–277
  34. Fick J, Ph D, Andersson PL et al (2004) Selection of antibiotics : a chemometric approach. In: 4th international conference on pharmaceuticals and endocrine disrupting chemicals in water, pp 143–150
  35. Wold SSM, Eriksson L, Sjöström M, Eriksson L (2001) PLS-regression: a basic tool of chemometrics. *Chemom Intell Lab Syst* 58:109–130. [https://doi.org/10.1016/S0169-7439\(01\)00155-1](https://doi.org/10.1016/S0169-7439(01)00155-1)
  36. Gramatica P, Cassani S, Roy PP et al (2012) QSAR modeling is not “Push a button and find a correlation”: a case study of toxicity of (Benzo-) triazoles on Algae. *Mol Inform* 31:817–835. <https://doi.org/10.1002/minf.201200075>
  37. Veith GD, Mekenyan OG (1993) A QSAR approach for estimating the aquatic toxicity of soft electrophiles [QSAR for soft electrophiles]. *Quant Struct Relationships* 12:349–356. <https://doi.org/10.1002/qsar.19930120402>
  38. Pavan M, Worth A, Netzeva T (2005) Comparative assessment of QSAR models for aquatic toxicity. European Communities, EUR 21750 EN
  39. Kuhn H, Braslavsky SE, Schmidt R (2004) *Chemical Actinometry*. IUPAC Technical Report, pp 1–47
  40. Hatchard CG, Parker C (1956) A new sensitive chemical actinometer. II. potassium ferrioxalate as a standard chemical actinometer. *Proc R Soc A Math Phys Eng Sci* 235:518–536. <https://doi.org/10.1098/rspa.1956.0102>
  41. Niessen WMA, Honing M (2015) Mass spectrometry strategies in the assignment of molecular structure: breaking chemical bonds before bringing the pieces of the puzzle together. *Struct Elucidation Org Chem Search Right Tools* 9783527333:105–144. <https://doi.org/10.1002/9783527664610.ch4>
  42. Schymanski EL, Singer HP, Slobodnik J et al (2015) Non-target screening with high-resolution mass spectrometry: critical review using a collaborative trial on water analysis. *Anal Bioanal Chem* 407:6237–6255. <https://doi.org/10.1007/s00216-015-8681-7>
  43. Niessen WMA (2011) Fragmentation of toxicologically relevant drugs in positive-ion liquid chromatography-tandem mass spectrometry. *Mass Spectrom Rev* 30:626–663. <https://doi.org/10.1002/mas.20332>
  44. Voigt M, Bartels I, Nickisch-Hartfiel A, Jaeger M (2019) Determination of minimum inhibitory concentration and half maximal inhibitory concentration of antibiotics and their degradation products to assess the eco-toxicological potential. *Toxicol Environ Chem*. <https://doi.org/10.1080/02772248.2019.1687706>
  45. Voigt M, Savelsberg C, Jaeger M (2018) Identification of pharmaceuticals in the aquatic environment using HPLC-ESI-Q-TOF-MS and elimination of erythromycin through photo-induced degradation. *J Vis Exp*. <https://doi.org/10.3791/57434>
  46. Voigt M, Bartels I, Nickisch-hartfiel A, Jaeger M (2018) Elimination of macrolides in water bodies using photochemical oxidation. *AIMS Environ Sci* 5:372–388. <https://doi.org/10.3934/envirosci.2018.5.372>
  47. Baghirzade BS, Yetis U, Dilek FB (2021) Imidacloprid elimination by O<sub>3</sub> and O<sub>3</sub>/UV: kinetics study, matrix effect, and mechanism insight. *Environ Sci Pollut Res* 28:24535–24551. <https://doi.org/10.1007/s11356-020-09355-2>
  48. Lavine BK, Ding T, Jacobs D (2010) LC-PDA-MS studies of the photochemical degradation of imidacloprid. *Anal Lett* 43:1812–1821. <https://doi.org/10.1080/00032711003654013>
  49. Elumalai P, Yi X, Cai T et al (2021) Photo-biodegradation of imidacloprid under blue light-emitting diodes with bacteria and co-metabolic regulation. *Environ Res* 201:111541. <https://doi.org/10.1016/j.envres.2021.111541>
  50. Fernandes CHM, Silva BF, Aquino JM (2021) On the performance of distinct electrochemical and solar-based advanced oxidation processes to mineralize the insecticide imidacloprid. *Chemosphere*. <https://doi.org/10.1016/j.chemosphere.2021.130010>
  51. Tian J, Rustum A (2018) Development and validation of a stability-indicating reversed-phase UPLC-UV method for the assay of imidacloprid and estimation of its related compounds. *J Chromatogr Sci* 56:131–138. <https://doi.org/10.1093/chromsci/bmx091>
  52. Wang Q, Rao P, Li G et al (2020) Degradation of imidacloprid by UV-activated persulfate and peroxymonosulfate processes: kinetics, impact of key factors and degradation pathway. *Ecotoxicol Environ Saf*. <https://doi.org/10.1016/j.ecoenv.2019.109779>
  53. Dell'Arciprete ML, Santos-Juanes L, Sanz AA et al (2009) Reactivity of hydroxyl radicals with neonicotinoid insecticides: mechanism and changes in toxicity. *Photochem photobiol Sci* 8:1016–1023. <https://doi.org/10.1039/b900960d>
  54. Babic K, Tomašić V, Gilja V et al (2021) Photocatalytic degradation of imidacloprid in the flat—plate photoreactor under UVA and simulated solar irradiance condition—The influence of operating conditions, kinetics and degradation pathway. *J Environ Chem Eng* 9:1–14. <https://doi.org/10.1016/j.jece.2021.105611>
  55. Joice JAI, Aishwarya S, Sivakumar T (2018) Nano structured Ni and Ru impregnated TiO<sub>2</sub> photocatalysts: synthesis, characterization and photocatalytic degradation of neonicotinoid insecticides. *J Nanosci Nanotechnol* 19:2575–2589. <https://doi.org/10.1166/jnn.2019.15880>
  56. Yin K, Deng Y, Liu C et al (2018) Kinetics, pathways and toxicity evaluation of neonicotinoid insecticides degradation via UV/chlorine process. *Chem Eng J* 346:298–306. <https://doi.org/10.1016/j.cej.2018.03.168>
  57. Žabar R, Komel T, Fabjan J et al (2012) Photocatalytic degradation with immobilised TiO<sub>2</sub> of three selected neonicotinoid insecticides: imidacloprid, thiamethoxam and clothianidin. *Chemosphere* 89:293–301. <https://doi.org/10.1016/j.chemosphere.2012.04.039>
  58. Sharma T, Kaur M, Sobti A et al (2020) Sequential microbial-photocatalytic degradation of imidacloprid. *Environ Eng Res* 25:597–604. <https://doi.org/10.4491/eer.2019.150>
  59. Agüera A, Almansa E, Malato S et al (1998) Evaluation of photocatalytic degradation of Imidacloprid in industrial water by GC-MS and LC-MS. *Analisis* 26:245–251. <https://doi.org/10.1051/analisis:1998168>
  60. Aregahegn KZ, Shemesh D, Gerber RB, Finlayson-Pitts BJ (2017) Photochemistry of thin solid films of the neonicotinoid imidacloprid on surfaces. *Environ Sci Technol* 51:2660–2668. <https://doi.org/10.1021/acs.est.6b04842>
  61. Garg R, Gupta R, Bansal A (2021) Photocatalytic degradation of imidacloprid using semiconductor hybrid nano—catalyst: kinetics,

- surface reactions and degradation pathways. *Int J Environ Sci Technol* 18:1425–1442. <https://doi.org/10.1007/s13762-020-02866-y>
62. Kitsiou V, Filippidis N, Mantzavinos D, Poullos I (2009) Heterogeneous and homogeneous photocatalytic degradation of the insecticide imidacloprid in aqueous solutions. *Appl Catal B Environ* 86:27–35. <https://doi.org/10.1016/j.apcatb.2008.07.018>
  63. Kurwadkar S, Evans A, DeWinne D et al (2016) Modeling photodegradation kinetics of three systemic neonicotinoids—dinotefuran, imidacloprid, and thiamethoxam—in aqueous and soil environment. *Environ Toxicol Chem* 35:1718–1726. <https://doi.org/10.1002/etc.3335>
  64. Moza PN, Hustert K, Feicht E, Kettrup A (1998) Photolysis of imidacloprid in aqueous solution. *Chemosphere* 36:497–502. [https://doi.org/10.1016/S0045-6535\(97\)00359-7](https://doi.org/10.1016/S0045-6535(97)00359-7)
  65. Redlich D, Shahin N, Ekici P et al (2007) Kinetic study of the photoinduced degradation of imidacloprid in aquatic media. *Clean - Soil Air Water* 35:452–458. <https://doi.org/10.1002/clen.200720014>
  66. Tang J, Huang X, Huang X et al (2012) Photocatalytic degradation of imidacloprid in aqueous suspension of TiO<sub>2</sub> supported on H-ZSM-5. *Environ Earth Sci* 66:441–445. <https://doi.org/10.1007/s12665-011-1251-1>
  67. Wamhoff H, Schneider V (1999) Photodegradation of imidacloprid. *J Agric Food Chem* 47:1730–1734. <https://doi.org/10.1021/jf980820j>
  68. Wang Y, Sun Q, Tian C et al (2016) Degradation properties and identification of metabolites of 6-Cl-PMNI in soil and water. *Chemosphere* 147:287–296. <https://doi.org/10.1016/j.chemosphere.2015.12.020>
  69. Zhang P, Shao Y, Xu X et al (2020) Phototransformation of biochar—derived dissolved organic matter and the effects on photodegradation of imidacloprid in aqueous solution under ultraviolet light. *Sci Total Environ* 724:137913. <https://doi.org/10.1016/j.scitotenv.2020.137913>

### Publisher's Note

Springer Nature remains neutral with regard to jurisdictional claims in published maps and institutional affiliations.

Submit your manuscript to a SpringerOpen<sup>®</sup> journal and benefit from:

- ▶ Convenient online submission
- ▶ Rigorous peer review
- ▶ Open access: articles freely available online
- ▶ High visibility within the field
- ▶ Retaining the copyright to your article

---

Submit your next manuscript at ▶ [springeropen.com](https://www.springeropen.com)

---